aerospace

MDPI

Article

A Systematic Qualification of a Planar-Type Phased Array Antenna with Cavity-Backed Slot Radiators for Communication Satellites Under Launch and On-Orbit Conditions

Hyun-Guk Kim [1], Jiye Bak [1], Seong-Ju Lee [2], Eun-Tae Jung [2], Woon-Sung Choi [2], Byeong-Gil Yu [2], Jaekark Choi [2], Jung-Il Cho [2,3], Won-Seok Lee [2], Insung Park [2], Hansol Min [2], Hyun Koh [2], Myeongjae Lee [1], Ji-Haeng Cho [4], Byeongjae Kim [4], Kyoung Youl Park [4], Kimin Hwang [4] and Ki Chul Kim [4,*]

[1] Satellite Mechanical Team, Hanwha Systems, 491-23, Gyeonggidong-ro, Namsa-myeon, Cheoin-gu, Yongin-si 17121, Republic of Korea; dpwl3984@hanwha.com (J.B.); myjae.lee@hanwha.com (M.L.)
[2] Satellite Payload Team 3, Hanwha Systems, 27 Hwangsaeul-ro 360beon-gil, Bundang-gu, Seongnam-si 13591, Republic of Korea; sungju1015.lee@hanwha.com (S.-J.L.); euntae.jung@hanwha.com (E.-T.J.); wschoi1011@hanwha.com (W.-S.C.); byunggil77.yu@hanwhasy.com (B.-G.Y.); jaekark.choi@hanwha.com (J.C.); jungil01.cho@hanwha.com (J.-I.C.); bestlee@hanwha.com (W.-S.L.); qkrdlstjd00@hanwha.com (I.P.); hsmin31@hanwha.com (H.M.); ktec829@hanwha.com (H.K.)
[3] Department of Integrated Space Defense, Yonsei University, 50 Yonsei-ro, Seodaemun-gu, Seoul 03722, Republic of Korea
[4] The 1st Research and Development Institute, Agency for Defense Development, Daejeon-si 34186, Republic of Korea; knowact@add.re.kr (J.-H.C.); bj6811@add.re.kr (B.K.); ky.park@add.re.kr (K.Y.P.); kiminida@add.re.kr (K.H.)
* Correspondence: kimkc@add.re.kr

Abstract

This paper presents a systematic qualification process for an electronic beam-steering antenna assembly for a low-Earth orbit (LEO) communication satellite. The transmitting/receiving antenna for the LEO communication satellite is based on a cavity-backed slot radiator, which has improved radiation efficiency and low mutual coupling compared to conventional PCB patch structures. In order to verify the electrical performance and reliability of the manual soldering process in a tightly spaced array structure with narrow element spacing and densely connected multi-channel RF modules, a reduced model was designed and fabricated and qualification tests were conducted under launch and on-orbit environments. The integration equipment was developed to ensure precise mechanical alignment and integration/disassembly between the radiating element arrays of the transmitting and receiving antenna modules and the RF modules, thereby establishing a manufacturability strategy for the antenna module and RF integrated module, which comprise a large array structure. Finally, the qualification tests of the transmitting and receiving antenna were performed to evaluate the structural and thermal stability considering the launch and orbital environments. The systematic qualification process proposed in this paper can be used in the development of the antenna system of the communication satellite.

Keywords: environment test; qualification; cavity-backed slot radiators; phased array antenna

Check for updates

Academic Editor: Mohammad Reza Soleymani

Received: 10 March 2026
Revised: 16 April 2026
Accepted: 29 April 2026
Published: 12 May 2026

Copyright: © 2026 by the authors. Licensee MDPI, Basel, Switzerland. This article is an open access article distributed under the terms and conditions of the Creative Commons Attribution (CC BY) license.

1. Introduction

The advent of the ICT revolution fueled by the contemporary digital transformation is driving a surge in global demand for satellite-based communications. The explosive growth in digital data demand driven by cloud computing, Internet of Things (IoT) devices, and the proliferation of remote work has created a situation where terrestrial networks alone

cannot meet the demand. Satellite communications are playing an increasingly crucial role, particularly in remote areas, maritime, and aviation where terrestrial communication infrastructure is unavailable. Furthermore, military/defense satellite communication requirements are also on the rise [1,2]. The small satellite communications market is expected to grow at a compound annual growth rate of 25.2% between 2025 and 2030, with the market size projected to increase from $5.95 billion in 2025 to $18.34 billion in 2030 [3]. This rapid growth is increasing the technological demand for the development of large-scale satellite constellations comprised of low-Earth orbit (LEO), medium-Earth orbit (MEO), and geostationary Earth orbit (GEO) satellites. The development of communication satellites goes beyond the simple design and construction of satellite platforms; it requires the implementation of highly reliable payload systems. Satellites are exposed to extreme vibration and shock during launch, as well as the extremely low temperatures and vacuum environments of orbit, requiring all electronic and mechanical equipment to operate reliably under these conditions. In particular, the antenna system, the core of the communication payload, is a key element in determining satellite reliability. Past incidents, such as SARah-Passiv, SkyTerra-1, and Viasat-3, which resulted in the total loss of multi-billion-dollar satellites due to antenna deployment failures, highlight the importance of proper design and certification [4,5].

An antenna system is a key payload for signal transmission between communication satellites and ground stations, and its design and performance determine communication performance, coverage, capacity, and reliability. Communication satellite antennas are primarily categorized by their intended use and frequency band. These include reflector antennas, which provide regional coverage; horn antennas, which possess high directivity; and phased array antennas, which enable electronic beam steering. Recently, phased array antennas with multi-beamforming capabilities have emerged as a core technology for next-generation satellite communication systems, enabling high-speed satellite tracking of LEO/MEO constellations and communications with terrestrial mobile systems (ships, aircraft, and vehicles) [6–8].

Phased array antennas are classified into linear arrays and planar arrays based on their configuration. Linear arrays have low manufacturing complexity but are limited to beam scanning in a single plane, whereas planar arrays can steer beams in both orthogonal planes, providing high flexibility and performance. In particular, planar phased array antennas can electronically steer beams by controlling the phase and amplitude of the signal through phase shifters arranged at each element and can achieve high reliability and lightweight design without the need for a mechanical drive device [9,10].

A cavity-backed slot-coupled patch antenna is a hybrid antenna structure that transmits signals through a slot placed behind a conductive cavity and places a microstrip patch radiating element on the slot. The ground plane provided by the cavity suppresses surface wave propagation and controls/confines the radiation directionality, while allowing free signal excitation through the slot [11]. Cavity-coupled slot patch antennas offer several significant advantages over conventional PCB-based microstrip patch antennas. The cavity structure effectively suppresses surface wave propagation, thereby improving radiation efficiency by 10–20%. This can improve the power efficiency of satellites. The metal wall of the cavity has the effect of reducing mutual coupling between array elements and homogenizing the impedance characteristics of the array elements, thereby reducing beam pattern distortion. By designing the internal structure of the cavity to utilize the dual resonance characteristics, it is possible to obtain both superior efficiency and gain while simultaneously broadening the impedance bandwidth, and the electromagnetic shielding characteristics of the cavity metal wall minimize electromagnetic interference with adjacent systems, which is very important in a high-density integrated satellite pay-

load environment [12,13]. During the manufacturing process of the antenna assembly, the transmit module and the receive module must be electrically connected to each antenna array element through fiber optic cables (for timing/control signals), RF connectors, and signal lines. In a large satellite antenna assembly with many antenna array elements, the reliability of these electrical connections determines the performance of the satellite's space mission. Manual soldering used in the manufacturing of the antenna assembly remains one of the most reliable methods with complex shapes and connection points located in narrow spaces, and it allows for better quality control than automatic soldering, especially for space electronic equipment that requires high reliability.

In space, solder joints are continuously exposed to extreme vibration during the launch phase, extreme thermal conditions in orbit, and high-energy particle radiation. Under these harsh environmental conditions, solder joints can crack due to thermal/mechanical fatigue. Therefore, assessing the reliability of solder joints goes beyond simple quality assurance and is essential to ensuring that satellites can operate without communication interruption throughout their designed mission. Space standards ECSS-Q-ST-70-08C and ECSS-Q-ST-70-38C require rigorous soldering process management, material qualification, and environmental stress testing to ensure this reliability [14,15].

Satellites are exposed to two extreme environmental conditions: launch and in-orbit operations. During the launch phase, the combination of rocket acceleration, acoustic vibration, and launch vehicle structural vibration generates extremely high dynamic stresses. NASA's General Environmental Verification Standard (GSFC-STD-7000A) and the European Space Standard (ECSS-E-ST-10-03C) specify severe vibration tests, including sinusoidal and random vibration, replicating launch environment conditions [16,17]. In the orbital environment, continuous temperature cycling, cryogenic temperatures, and high vacuum (less than 10^{-5} Pa) are experienced throughout a mission. These cyclical temperature changes induce thermal stresses between components with different coefficients of thermal expansion, and long-term accumulated fatigue significantly reduces the reliability of mechanical components and electronic joints [18,19].

In this study, a systematic qualification test was conducted for large-scale phased array antenna assemblies, namely transmitting and receiving antenna assemblies with large-scaled array. A transmitting (36-element) and a receiving (48-element) reduced model of two antenna assemblies were fabricated and thermal cycling tests were performed, considering launch and orbital conditions. Qualification tests for the reduced model were primarily conducted to verify the reliability of manual solder joints and, if there are any issues, provides an opportunity to improve the process before full-array fabrication. Assembly support equipment was designed and manufactured to precisely align and assemble the antenna and RF modules with fully arranged layout. Final qualification testing was performed on the full-array transmitting and receiving antenna assemblies, with the structural environmental, thermal cycling/vacuum, and shock tests as a qualification process. The radiation pattern, gain, and impedance characteristics were measured before and after each qualification test to evaluate the performance degradation of the electrical function. The qualification process for the communication satellite antenna developed in this study can serve as a reference for the development of future communication satellite antennas.

2. Overview of Ka-Band LEO Communication Satellite

LEO satellites operate at altitudes of approximately 500–2000 km above the Earth's surface, with a minimum distance to the Earth's surface that is only about 1/72 that of geostationary orbit (GEO) satellites [20]. This short-range characteristic significantly reduces signal attenuation and shortens the round-trip time to approximately 50 ms, enabling low-latency communication. Furthermore, LEO satellites can form constellations

of tens to thousands to provide full global coverage, enabling communication services in all areas where existing terrestrial networks are not available, such as maritime, aerial, polar, and remote areas. Another key advantage of LEO constellations is network resilience. Inter-satellite links (ISL) enable communication with satellites that are inaccessible to ground stations, and even in the event of a satellite failure, other satellites compensate for the failure, ensuring service continuity [20].

The Ka-band (26.5–40 GHz) uses a much higher frequency than the Ku-band (12–18 GHz) or L-band (1–2 GHz), allowing for a capacity increase of about 10 times or more within the same bandwidth [21]. Ka-band communications enable wide bandwidth communications, allowing for faster transmission of more data, making it ideal for high-speed Internet, HD and 4K video streaming, and real-time data downlinks. Since the antenna gain is proportional to the square of the frequency, the same signal strength can be achieved with a smaller antenna, enabling lightweight and compact satellites. Meanwhile, in LEO constellations, inter-satellite link communications are a key technology for securing both network autonomy and global coverage. Figure 1 shows the conceptual diagram of communication satellite system. Each satellite forms an ISL with two to four neighboring satellites within the same orbital plane and satellites in adjacent orbital planes, forming a grid-shaped satellite network. Data is transmitted via optical ISL or RF links between satellites, even in areas inaccessible to ground stations. ISL capacity is rapidly evolving from tens of Mbps based on existing RF to tens to hundreds of Gbps based on optical communications, enabling real-time information sharing and autonomous network operation among satellite constellations [22].

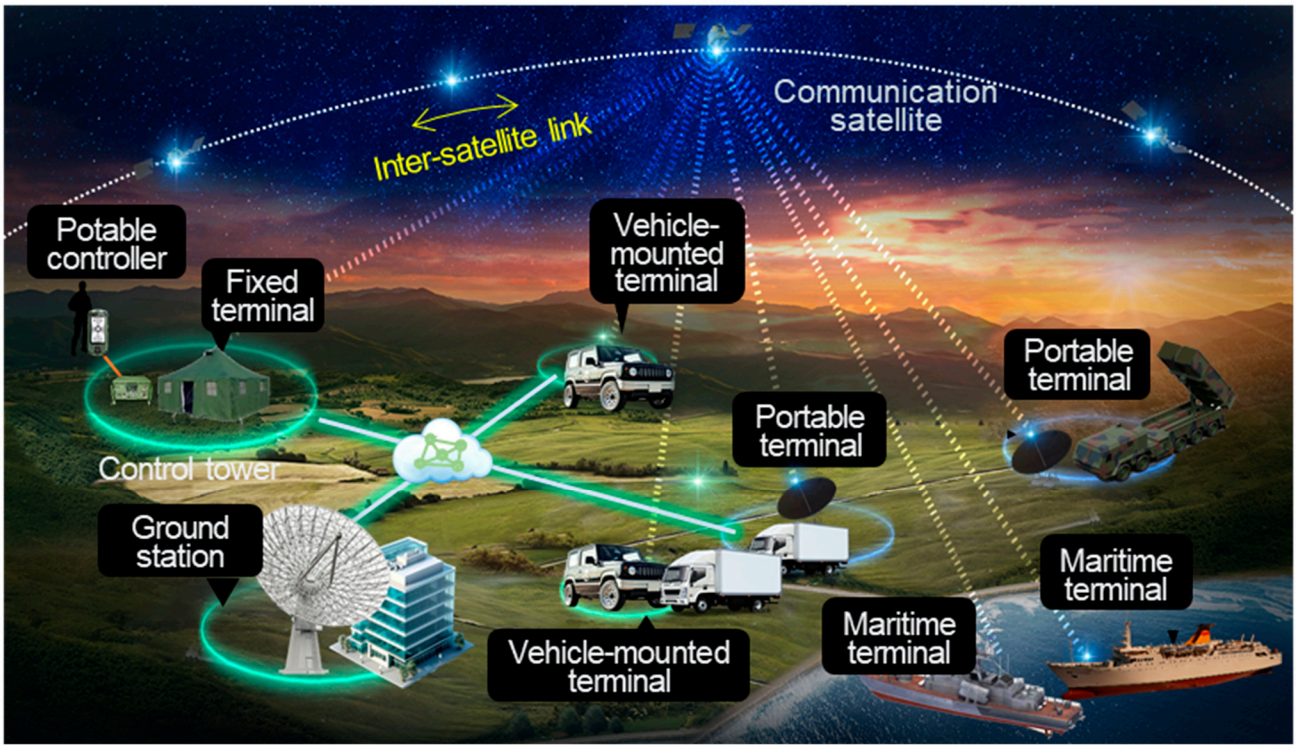


Figure 1. Conceptual diagram of communication satellite system.

Beam steering is a necessary requirement in LEO satellite systems using the Ka-band. LEO satellites have orbital periods of approximately 100 min, resulting in a severely limited communication window with the ground. Furthermore, the satellite's high-speed movement rapidly changes the signal reception point. Therefore, a fixed beam alone cannot maintain a stable link with fast-moving ships, aircraft, and vehicles on the ground.

Electronic beam steering is required to change the direction of signal transmission without mechanical movement [23,24]. Furthermore, since a single satellite must be able to communicate with multiple ground stations simultaneously through multi-beam-forming capabilities, the development of an electronic beam-steering antenna capable of independently controlling the phase and amplitude of each array element is essential.

From this perspective, this study designed a planar phased array antenna system, arranging antenna elements on a two-dimensional plane. This system can simultaneously steer beams in both elevation and azimuth directions and is optimized for effectively tracking fast-moving ground targets across a wide field of regard. Therefore, a phased array antenna consisting of the fully arranged transmitting and receiving antenna assemblies was fabricated, resulting in the construction of a Ka-band low-Earth orbit communication satellite system.

3. Qualification of Manual Soldering in Reduced Module of Transmitting/Receiving Antenna Assembly

In this section, we developed a 36-element scale model of a transmit antenna assembly and a 48-element scale model of a receive antenna assembly to systematically evaluate the reliability of the manual soldering process. Step-by-step verification using scale models follows the "Qualification Testing" philosophy of the European Space Agency (ESA) standard ECSS-E-ST-10-03C. By experiencing the harsh environmental conditions of launch and orbital operation in advance, we provide opportunities for early detection of design flaws and process improvement prior to full-scale antenna fabrication. Specifically, the scale models replicate the basic structure of the transmit/receive antenna assemblies, the arrangement of array elements, and the interconnection of phase shifters and feeder networks, ensuring representativeness while reducing the time and cost required for reliability testing. Furthermore, failure mode analysis, threshold data, and information on solder joint fatigue mechanisms obtained through environmental testing of the scaled models are directly utilized in the subsequent antenna assembly process. The reliability assessment of the scaled-down model of the antenna module was performed following a sequential environmental stressing procedure of vibration test → shock test → thermal cycle test, and both structural integrity and electrical performance were verified before and after each test. In the vibration test stage, broadband random vibration of 20–2000 Hz based on NASA GEVS standard was applied to simulate the acoustic vibration and mechanical excitation force of the launch stage, and the changes in the frequency response function (FRF) and resonant frequency before and after each full-level test were measured to detect structural damage or cracks in the solder joints at an early stage. The shock test stage simulates the impact load of the separation mechanism and the high-frequency ringing of the rocket structure. After the test, the scattering parameters (S-parameters), including the reflection loss and transmission characteristics, are measured to confirm that there are no electronic changes that affect the antenna's impedance matching and gain. The thermal cycling test stage applies repetitive temperature changes on the track to induce cumulative thermal fatigue between components (package, substrate, solder) with different coefficients of thermal expansion (CTE), and the RF performance is continuously monitored after each cycle. Finally, after all environmental tests are completed, optical microscopy is performed through micro-section cross-section cutting to verify the extent of cracks, voids, and intermetallic compound (IMC) growth inside the solder joint, and to confirm the reliability of the soldering process itself.

3.1. Environment Test of the Reduced Model Considering the Strucutral and Thermal Conditions

In this chapter, we conduct a qualification test for the soldering process from a structural/thermal perspective. Table 1 shows the specifications for the sine vibration, random vibration, shock, and thermal cycle tests used for the qualification test of the reduced model manual soldering process for the transmitting and receiving antenna module. The qualification test specifications for the manual soldering process certification follow the specifications of the ECSS-Q-ST-70-08C standard document [14]. The sine vibration test, random vibration test, and shock test are performed by applying a load in each direction once according to the test specifications. Before and after each vibration test, the frequency response characteristics are measured using a low-level sine-sweep-test-based mode search to evaluate changes in the first-mode characteristics and identify any structural changes. As mentioned in Figure 2c, after evaluating the mode characteristics, a visual inspection is performed, and passive return loss is measured to identify any functional changes in the PCB and soldering. In the impact test, the reduced model is subjected to a single load in each direction, and the aforementioned functional/performance test is performed after each axis test. Finally, the thermal cycle test with 500 cycles is performed, divided into two phases of 200 and 300 cycles. A functional/performance evaluation is performed between Phase 1 and Phase 2 to determine whether the test is pass or fail, and the final functional/performance test is performed after Phase 2. Finally, a micro-section test is performed to observe the presence or absence of solder joint defects and to conduct a test for process certification.

Table 1. Test specification of the soldering qualification of the reduced models for the transmitting/receiving antenna.

Test	Direction	Frequency [Hz]	Value	Remarks
Sine vibration test	All directions	25~100 100~200	25 g 15 g	Sweep rate: 1 octave/min
Random vibration test	Parallel to PCB	20~100 100~800 800~2000	+6 dB/octave 0.5 g^2/Hz −3 dB/octave	Overall 27.1 g Duration: 5 min
	Perpendicular to PCB	20~100 100~500 500~2000	+6 dB/octave 1.0 g^2/Hz −6 dB/octave	Overall 28.5 g Duration: 5 min
Low-level random vibration test	All directions	5~2000	0.0005 g^2/Hz	Overall 1 g Duration 1 min
Shock test	All direction	100~550 550~4000	40 g 200 g	1 time for each direction
Thermal cycle test	-	-	−55~100 °C	Dwell time: 15 min 500 cycles

Figure 3 shows the results of the sine vibration test and the random vibration test. In both vibration tests, feedback control is performed using the control sensor to apply the excitation force that meets the test specifications to the specimen, and the response of the control sensor is used to evaluate whether the test was performed according to the qualification specifications shown in Table 1. Figure 3a,b show the responses of the control sensor measured in the sine vibration test of the transmitting reduced model and receiving reduced model of the antenna module, and Figure 3c,d show the results of the random vibration test. The responses of the control sensor measured in the sine vibration test and the random vibration test indicate that the scale model test of the transmitting and receiving antennas was performed with an appropriate load compared to the test specifications [25].

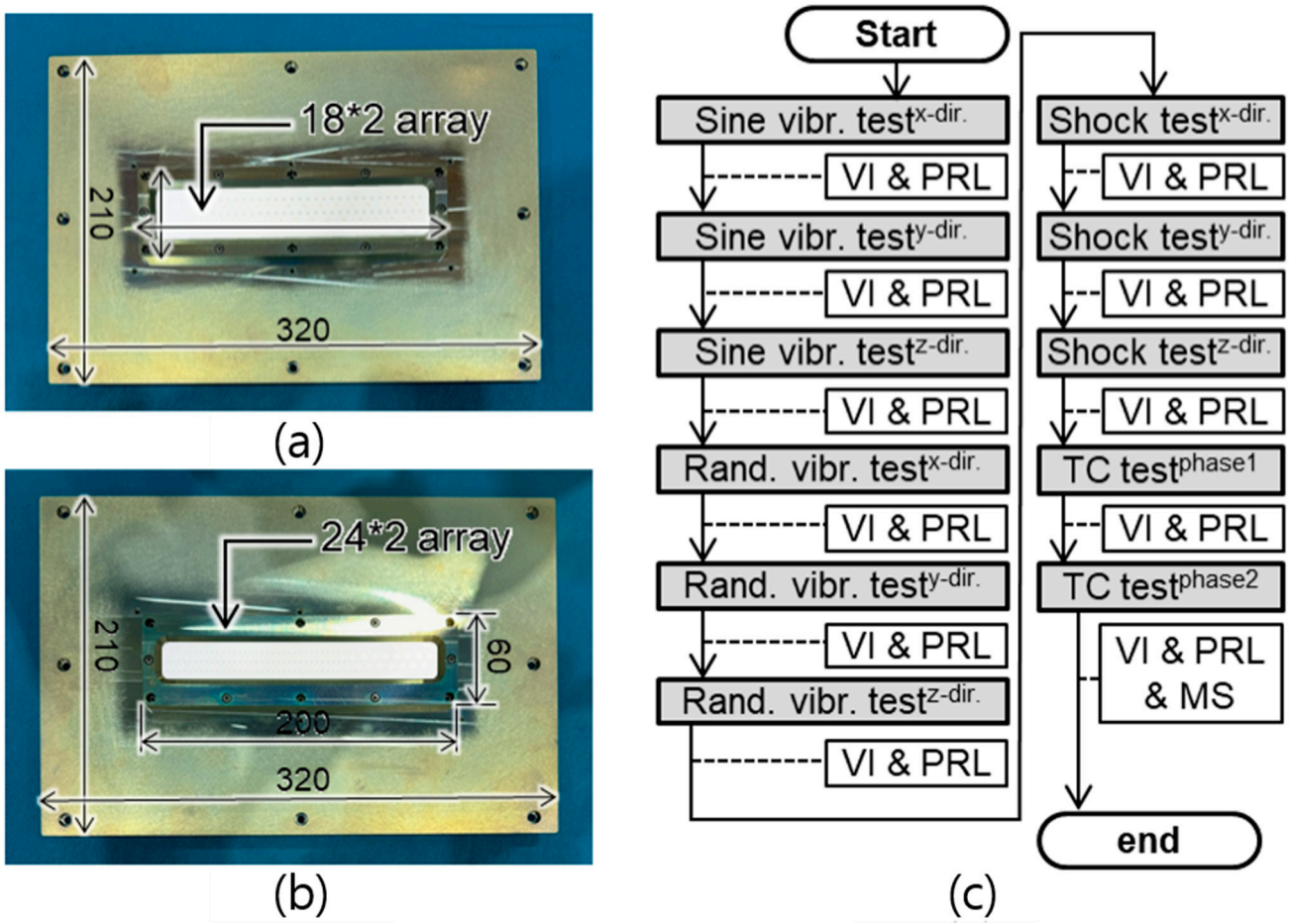


Figure 2. Reduced model and qualification test procedure: (**a**) Transmitting reduced model (TRM); (**b**) receiving reduced model (RRM) of antenna module; and (**c**) qualification procedure of the manual soldering process used to manufacture the cavity-backed slot radiator with the sine vibration, random vibration, shock, thermal cycling (TC) test. Visual inspection (VI) and a passive return loss (PRL) is measured between each test; a microsection (MS) of the soldering joint is investigated at the last stage.

Figure 4 shows the shock test results for the transmitting reduced model and the receiving reduced model for the antenna module. As with the vibration test, an accelerometer is attached to ensure that the shock force meets the test specifications. However, since the shock load is a one-time excitation, not an alternating load like in the vibration test, a one-way control method is used instead of a closed-loop control method. This method repeatedly applies shocks and compares the SRS responses measured from the accelerometer to determine the shock tester excitation conditions that meet the test specifications. Figure 4a,b show the experimental setups for horizontal and vertical shock tests on the two reduced models. When conducting shock tests with a shock tester, the operator can adjust shock test conditions such as the weight of the dropping weight or the angle of the arm. Using the excitation conditions derived from the operator's technical intuition and experience, only one shock force is applied to each direction. The reference response measured from the control sensor during the shock test is compared with the specifications defined in Table 1 to determine the pass/fail criteria for the test. Figure 4c shows that the impact tests of the two reduced models were conducted normally in accordance with the test specifications.

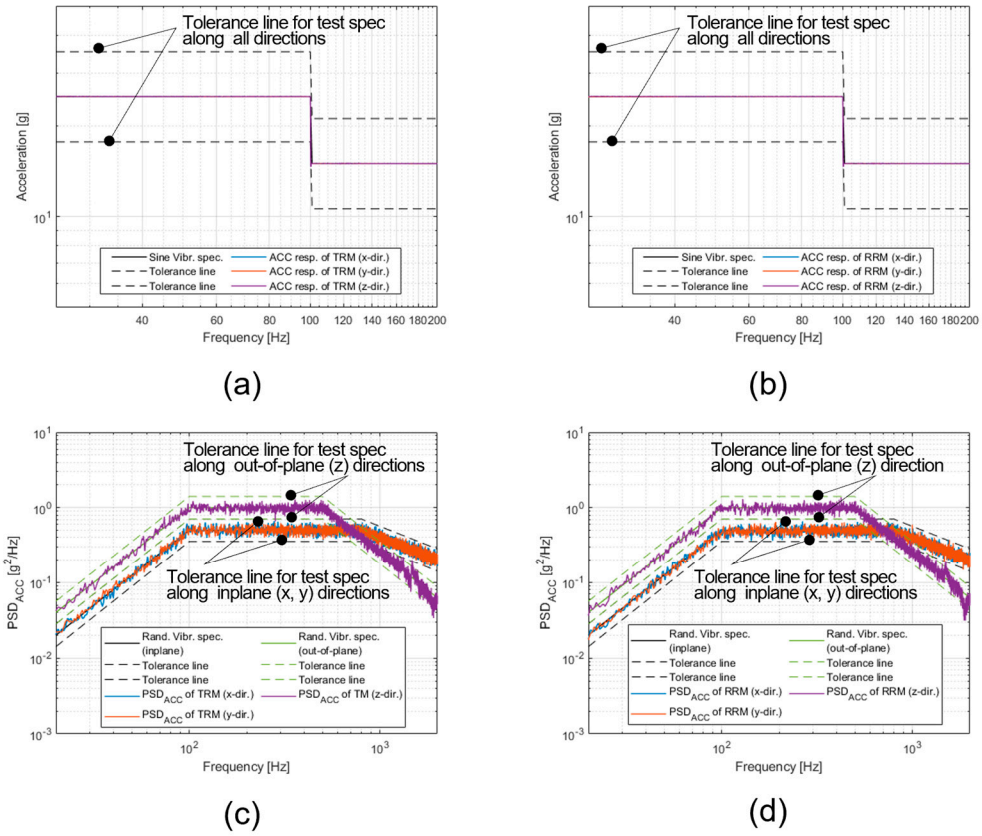


Figure 3. Result of sine vibration and random vibration tests: Reference response of control sensor measured by the sine vibration test of the (**a**) transmitting reduced model (TRM) and (**b**) receiving reduced model (RRM); control sensor measured by random vibration test of (**c**) TRM and (**d**) RRM.

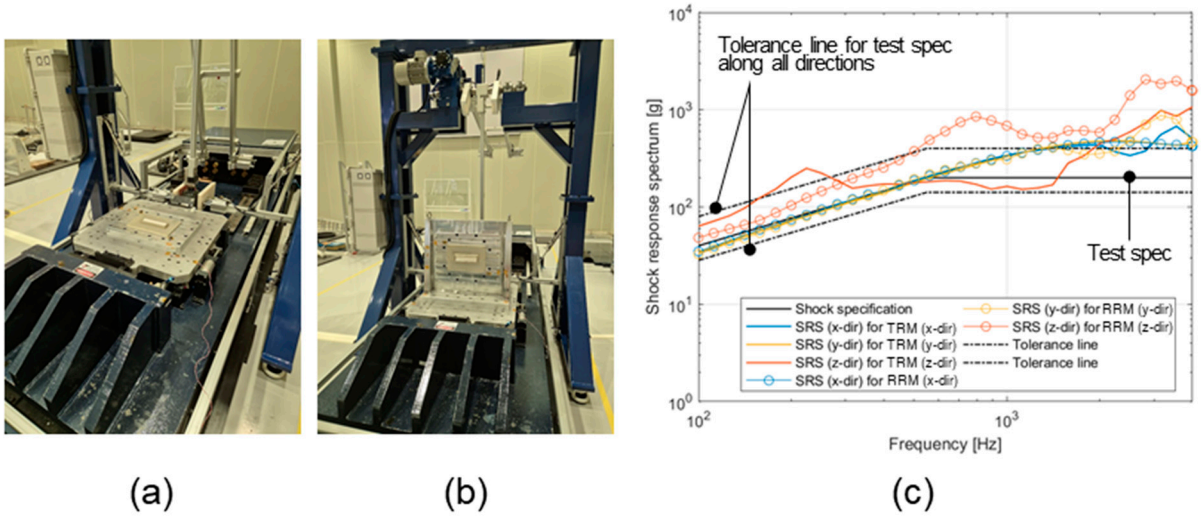


Figure 4. Result of shock test of the reduced model for transmitting reduced model (TRM) and receiving reduced model (RRM): Experimental setup for (**a**) horizontal and (**b**) vertical directions of two modules; (**c**) shock response spectrum (SRS) response of TRM and RRM for each direction.

Figure 5 shows the thermal cycle test results for the transmitting reduced model and receiving reduced model of the antenna module. Because the certification standards for the manual soldering process defined in Table 1 do not consider vacuum, thermal cycle testing was conducted in a temperature chamber capable of creating high and low temperature environments under atmospheric pressure. According to the ECSS standard document, 500 cycles were tested to verify the soldering process [14]. The thermal cycle test was

divided into Phase 1 (200 cycles) and Phase 2 (300 cycles). Between Phases 1 and 2, a visual inspection of the solder joint was performed, and the passive return loss of both reduced models was measured to determine whether to continue the thermal cycle test. As defined in Table 1, the test temperatures for both reduced models ranged from −55 to +100 °C, with a dwell time of 15 min for each cycle at both high and low temperatures. The temperature histories in Figure 5 demonstrate that the thermal cycle test of the reduced models of the transmitting and receiving antennas was conducted in compliance with the standards.

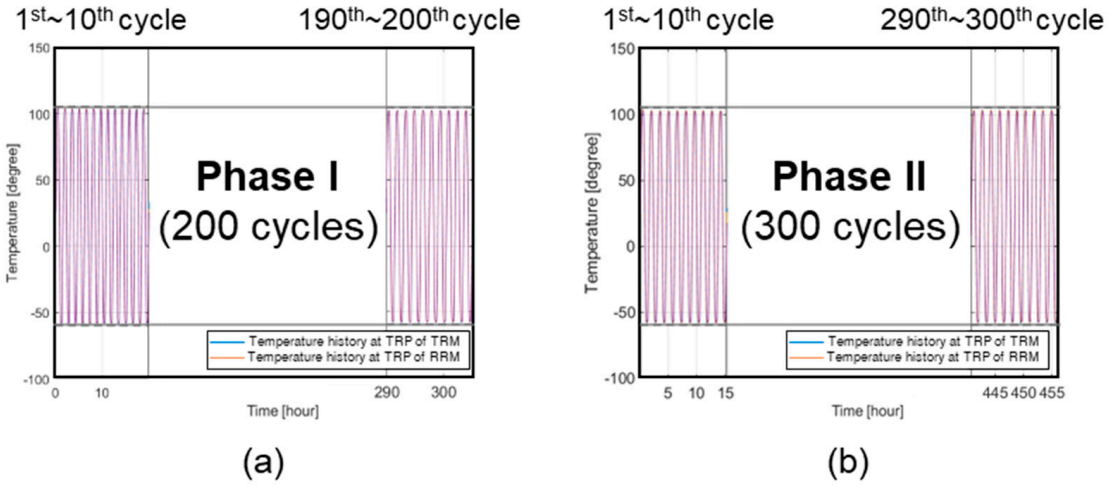


Figure 5. Result of thermal cycling test of the reduced model for transmitting module (TM) and receiving module (RM): Temperature history measured during (**a**) phase 1 (300 cycles) and (**b**) phase 2 (200 cycles).

3.2. Evaluation of Function and Performance of the Reduced Model of Transmitting and Receiving Antennas Assembly

As mentioned in Figure 2c, before and after each test, visual inspection and manual return loss measurements were performed to assess the presence of functional/performance defects in the scale model of the transmit/receive antenna assembly. A visual inspection using a magnifying glass revealed any visible defects in the solder and bullets of the scale model of the transmit/receive antenna section. As shown in Figure 6, the visual inspection revealed no defects in the solder or bullets.

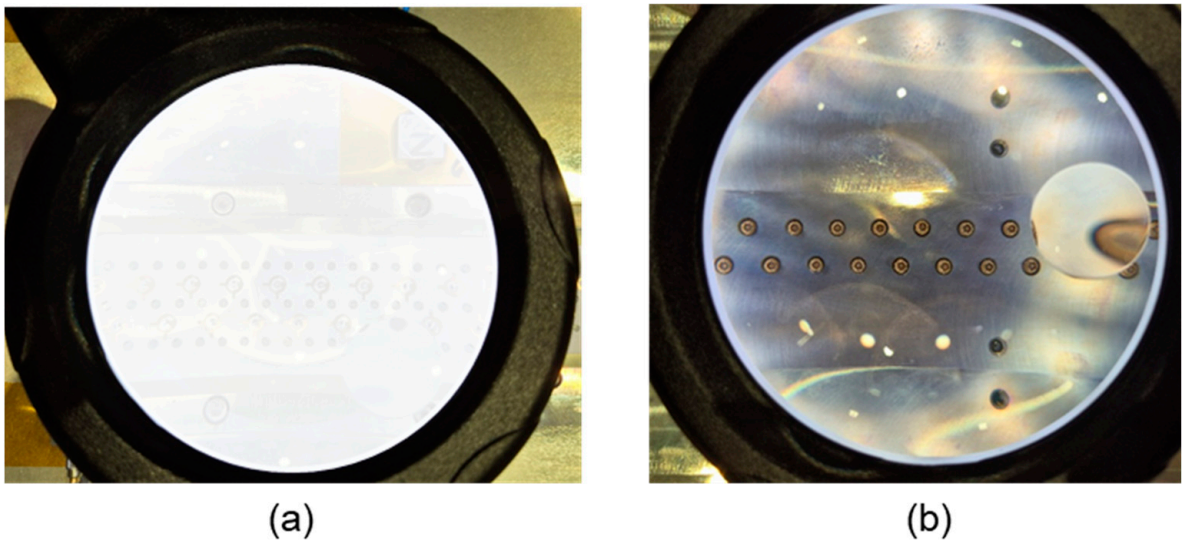


Figure 6. Result of visual inspection for the reduced model of antenna module to evaluate the mechanical defect on (**a**) upper side (soldering part) and (**b**) lower side (bullet side).

Figure 7 shows the results of the passive return loss measurement test of the antenna. Using the setup in Figure 7a, the passive return loss of the scaled-down model of the antenna section can be determined to verify whether the impedance matching is properly maintained at the antenna feed port, and whether any mismatch has occurred in the feed section, solder joint, and wiring due to mechanical load and deterioration after vibration, shock, and thermal cycle tests. In the passive return loss measurement test, the return loss of each scaled-down model was measured to verify that the value was maintained below 00 dB in the frequency range of the Ka-band. Figure 7b,c show that the return loss measured from the scaled-down models of the passive and active antennas, respectively, after the thermal cycle test, which is the final test of the soldering qualification, showed values below 10 dB.

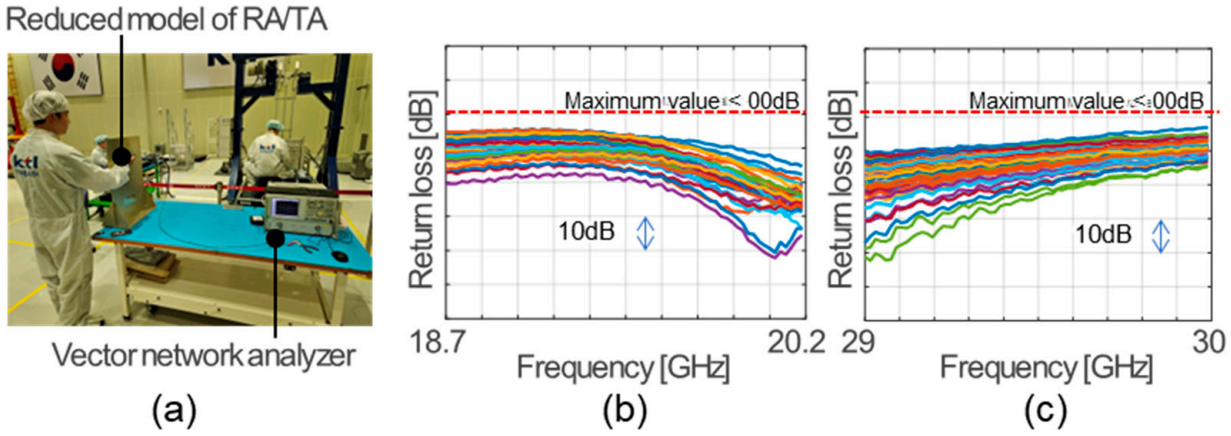


Figure 7. Result of passive return loss (PRA) of the reduced model for transmitted antenna (TA) and receiving antenna (RA) using the vector network analyzer: (**a**) Experimental setup to measure PRA; return loss of the reduced model for (**b**) TA and (**c**) RA.

Figure 8 shows the results of a microsection test. This test involves directly observing the internal cross-section of a solder joint to identify defects such as solder spread, cracks, delamination, and wetting after performing vibration, shock, and thermal cycle tests to certify the soldering process used in the antenna reduced model. Microsection analysis was conducted on the solder joints using an optical microscope equipped with a calibrated stage micrometer to assess structural integrity and measure key dimensional parameters. Cross-sectional specimens were prepared through standard metallographic procedures—including mounting, grinding, and polishing—and subsequently examined for failure modes such as cracking, delamination, and voids, while solder fillet dimensions and fill percentage were quantitatively measured against the calibrated reference scale. During the process qualification test, the solder joint experiences extreme dynamic loads and temperature cycles, which can often lead to internal fatigue cracks. In this work, a microsection test was conducted for each 10 solder joints of the two reduced models. Because these internal cracks are difficult to detect through visual inspection or electrical testing alone, the microsection test was performed as the final step in the solder joint process qualification test. Figure 8 shows one of the cross-sections of the solder joint as a result of the microsection test.

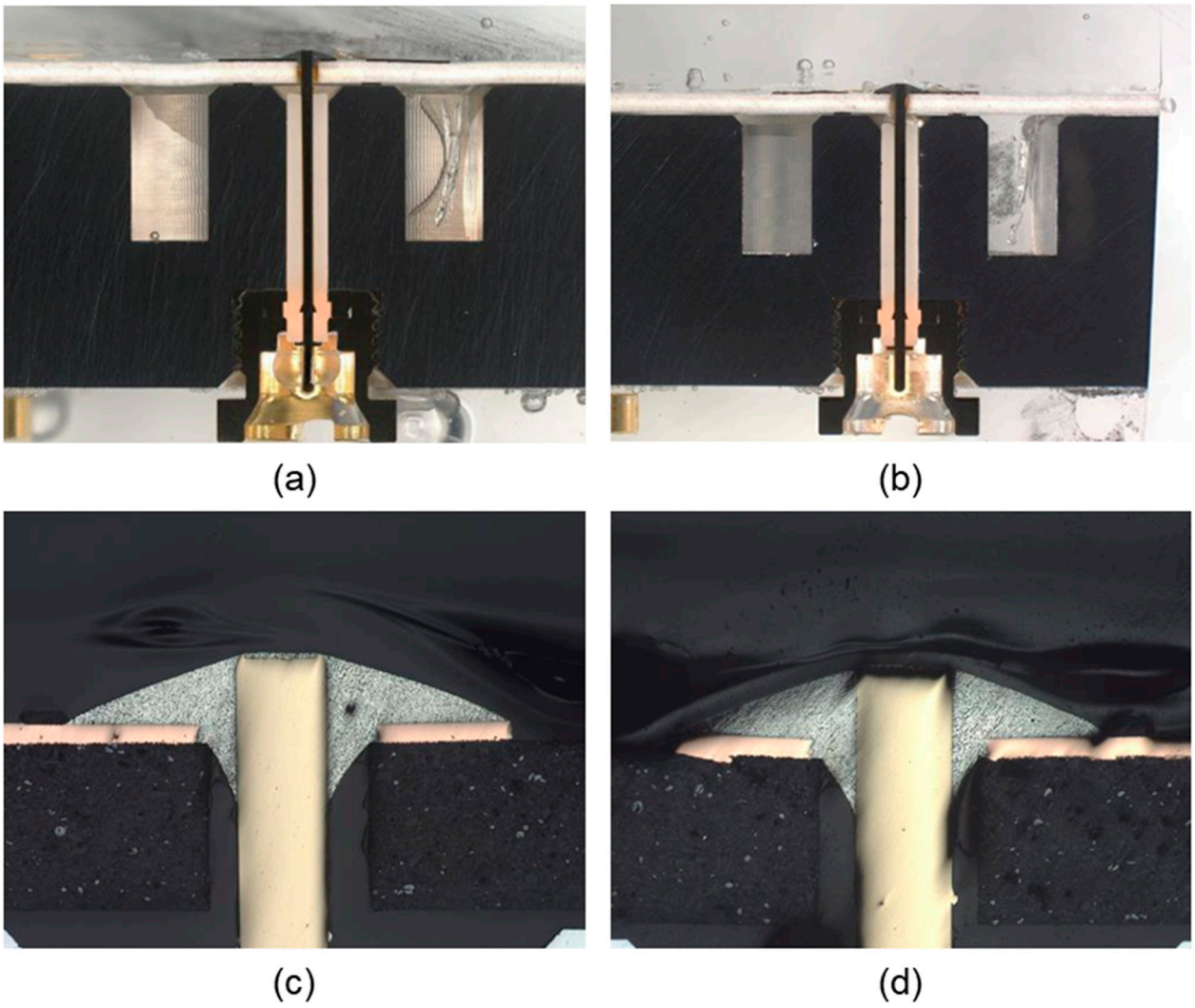


Figure 8. Result of the microsection test; example of cross-section in the transmitting reduced model (TRM) and receiving reduced model (RRM); zoomed view (×50) of (**a**) TRM and (**b**) RRM; detailed zoomed view (×150) of (**c**) TRM and (**d**) RRM.

4. Assembly and Integration of the Antenna and RF Assemblies

This section covers the assembly/integration process of the antenna assembly and the RF integrated assembly. The antenna assembly, based on the cavity-backed slot-type radiator proposed in this study, is connected one to one with the RF assembly using bullets. As shown in Figure 9, the antenna assembly consists of a combination of an antenna module and an RF integrated module. Unlike unit structures that can be assembled manually, transmitting and receiving antennas for communication satellites consist of arrays of over 200 antennas, requiring a significant load during assembly. Furthermore, since the cavity-backed slot-type radiator-based antenna is attached to the PCB, excessive load can cause damage to the PCB and solder joints.

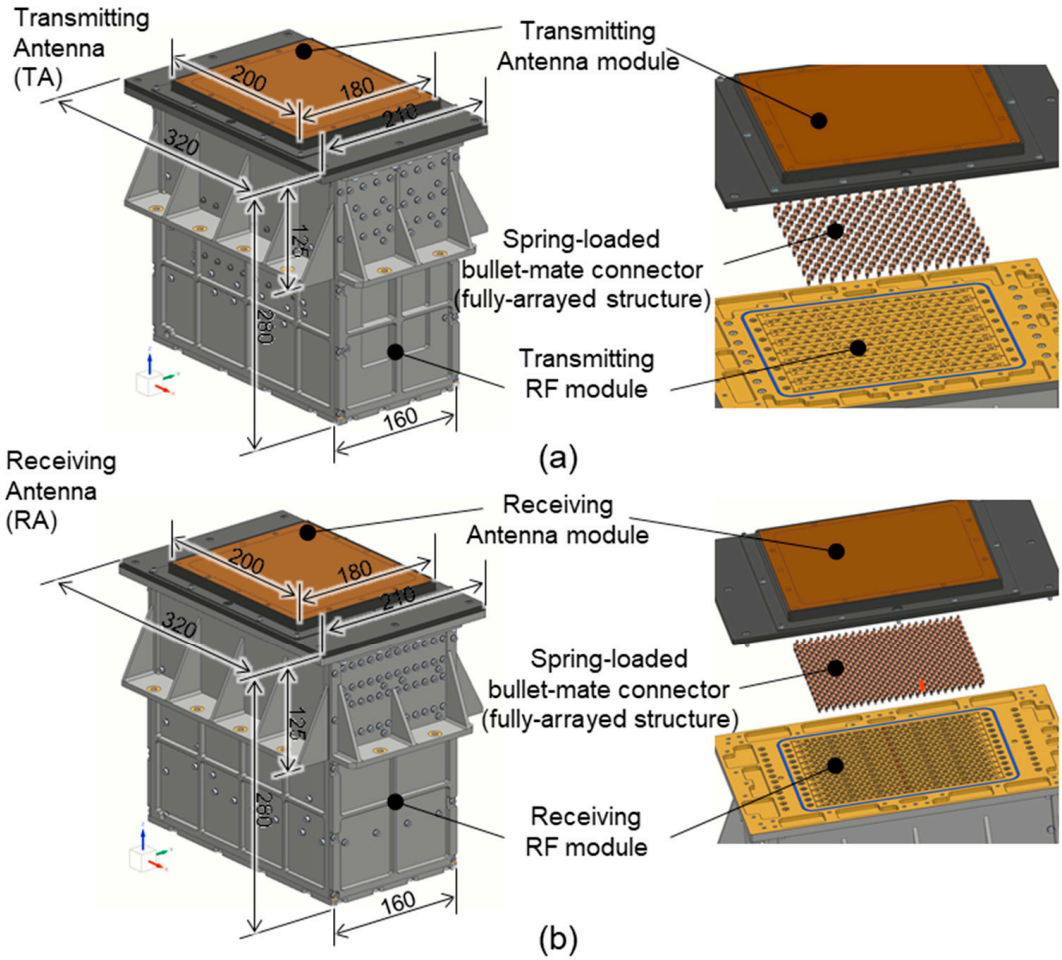


Figure 9. Conceptual layout of the (**a**) transmitting antenna Assembly (TAA) and (**b**) receiving antenna Assembly (RAA), consisting of RF and antenna modules. Exploded views show the configuration of the antenna assembly consisting of antenna module, RF module and spring-loaded bullet-mate connector.

In this regard, this chapter develops the mechanical ground support equipment (MGSE) for assembly and integration for assembling an antenna module and an RF module. The MGSE, designed for the assembly and integration of the antenna assembly shown in Figure 10, consists of a clamping plate capable of applying uniform pressure to the antenna's PCB surface without physical scratches; a guide rail and guide pins that ensure the antenna module can be attached to the RF module while maintaining a horizontal position; and a support structure that protects the connector at the bottom of the RF module and maintains it in a vertical position. As shown in Figure 9, since the physical dimensions of the transmitting antenna assembly (TAA) and receiving antenna assembly (RAA) are identical and the types and locations of the fastening holes used for physical connection with the satellite are the same, the assembly and integration are performed using the same MGSE for RAA and TAA. Also, the structural environment test and shock test zig are also identical for TAA and RAA.

Figure 11 illustrates the process of assembling the transmitting antenna assembly and the RF transmitter assembly. First, the RF assembly is attached to the supporting structure to create a vertically standing position, and the guide pin and guide rail are installed. The guide pin is used to maintain the antenna module's horizontal position during assembly, and a press plate is installed to apply even pressure to the PCB. Next, bolts are fastened to each fastening hole, and the antenna module and RF module are fastened while rotating

the assembly by one pitch while maintaining the horizontal position. Finally, the guide pin and guide rail are removed from the antenna assembly to complete the assembly process.

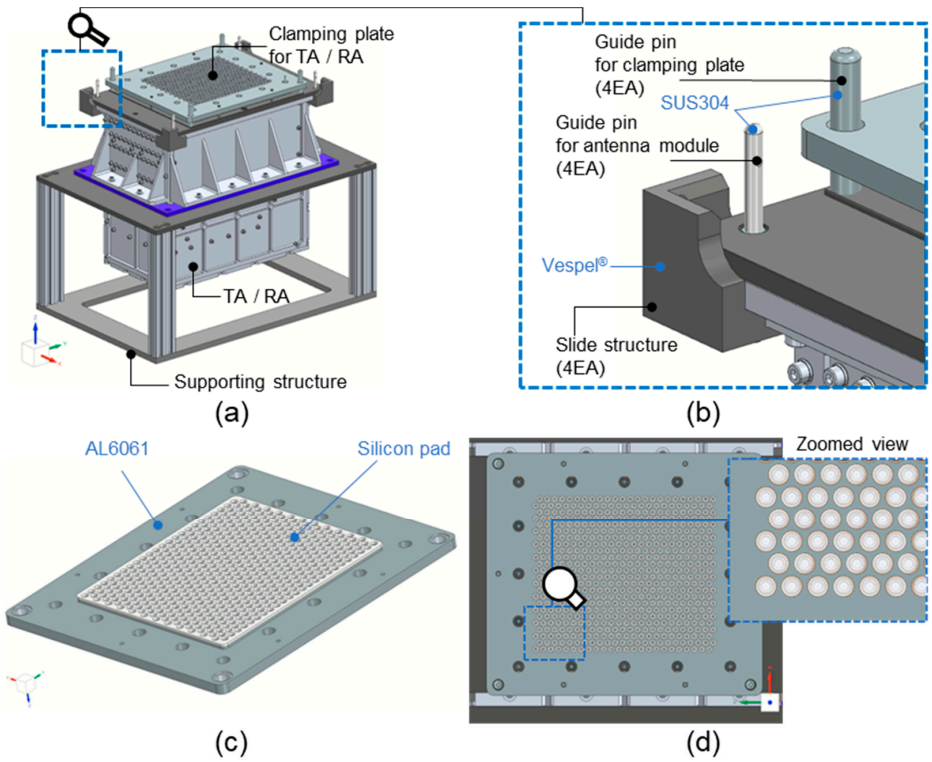


Figure 10. Mechanical ground support equipment for assembly and integration of antenna and RF assemblies: (**a**) Integration equipment; (**b**) zoomed view to present the guide rail and guide pin; (**c**) clamping plate consisting of the aluminum panel and silicon plate; (**d**) top view of the clamping plate to push the PCB plate with uniform pressure avoiding solder joints.

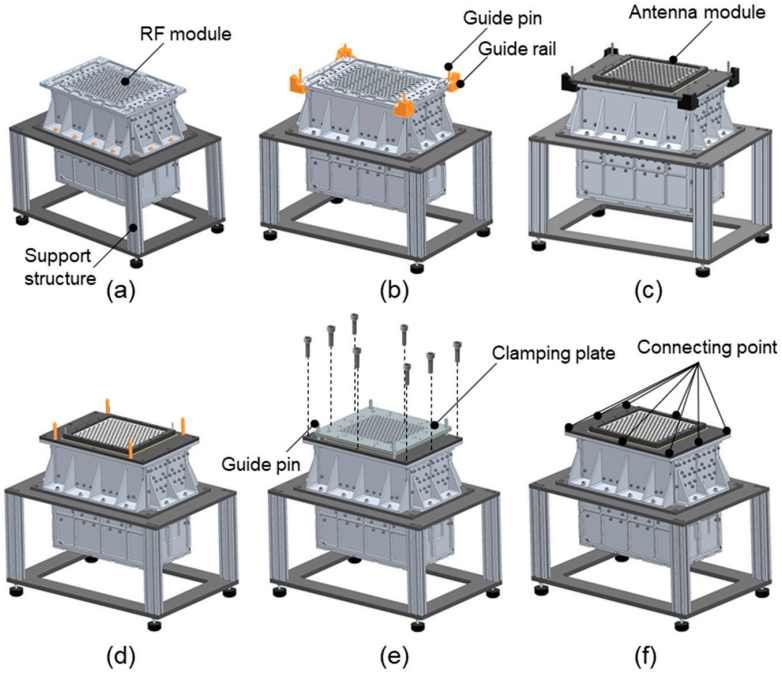


Figure 11. Procedure of assembly and integration of the transmitting antenna assembly (TAA) consisting of transmitting antenna module and RF transmitting module (the procedure of the receiving

antenna (RA) is same with TA): (**a**) RF module equipped on the support structure; (**b**) guide pin/rail to facilitate the vertical movement of the antenna module; (**c**) step in pre-assembly of the antenna module on the RF integrated module, aligned guide pin and rail; (**d**) step in assembly of the antenna module using the clamping plate to uniformly distribute load across the upper surface, while fasteners are rotated synchronously to maintain horizontal condition; (**e**) step in removal of guide rain/pin and clamping plate; (**f**) last step in removal of fastener between TAA and MGSE. It is possible to use this procedure in the assembly of RAA.

5. Qualification of Transmitting/Receiving Antenna Assembly

This section performs qualification of the integrated transmitting and receiving antenna sections from the previous section. Figure 12 illustrates the qualification procedure for the entire transmitting and receiving antenna section model. The structural integrity of the antenna assembly is verified through vibration testing using a vibration exciter, subjected to quasi-static acceleration and sine/random vibration. After completing environmental testing for each axis, a health check, a minimal functional/performance test, is performed to verify the functional survivability of the antenna assembly before moving on to the next axis. The thermal test consists of a one-cycle thermal cycling test and an eight-cycle thermal vacuum test. For the thermal cycle test, a health check is performed after each test to determine the survivability of the certified model of the transmitting and receiving antenna sections. Finally, a shock test is performed on both antenna assemblies. As with the reduced model of the antenna module, a single shock is applied in each direction to minimize the accumulated shock load on the prototype. The pass/fail status of the shock test is determined through a functional/performance test. The thermal cycle and thermal vacuum tests for the two antenna assemblies were conducted simultaneously because they had the same specifications, and other environmental tests were conducted separately for the transmitting antenna section and the receiving antenna section.

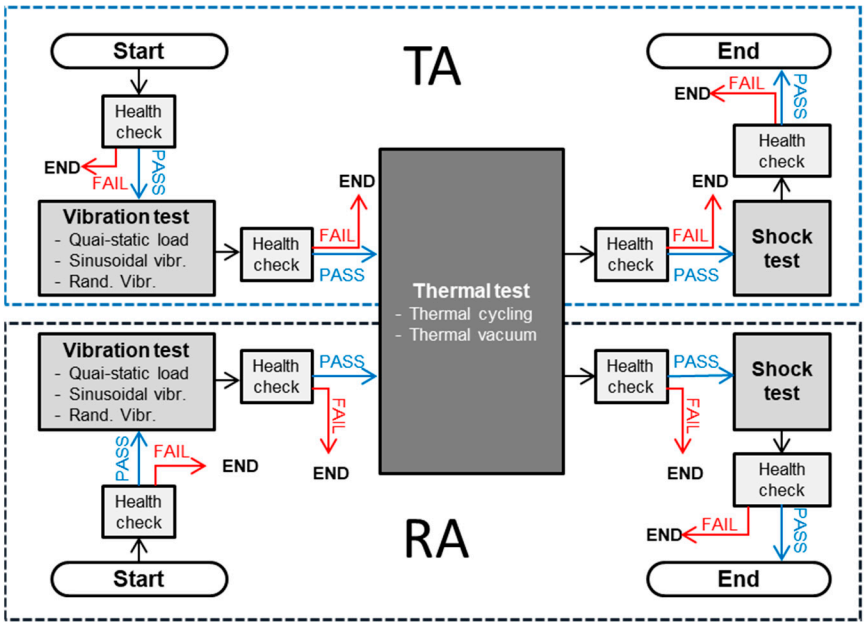


Figure 12. Qualification procedure of transmitting antenna (TA) and receiving antenna (RA) considering structural environment, thermal condition and shock load.

Table 2 presents the qualification test specifications for the transmitting and receiving antenna assemblies. Structural environmental tests confirmed the structural integrity of both antenna assemblies under quasi-static, sinusoidal, and random vibration loads. Thermal vacuum and thermal cycle tests of the antenna assemblies verified their ability to

withstand orbital environments, while impact tests confirmed the prototype's survivability against impact loads caused by activities such as stage separation and solar panel ejection. All qualification tests conducted in this paper were performed in accordance with the test specification derived from the system-level analysis of the satellite.

Table 2. Test specification of the qualification of the transmitting antenna (TA) and receiving antenna (RA).

Test		Direction	Frequency [Hz]	Value
Frequency requirement		All directions	-	≥150 Hz
Sine burst test	TA	All directions	20 Hz	≈30 g
	RA	All directions	20 Hz	≈30 g
Sine vibration test	TA/RA	All directions	25~100 100~200	20 g 6 g
Random vibration test	TA	Horizontal	20~100 100~300 300~2000 Overall	+6 dB/octave 00 g^2/Hz −3 dB/octave ≤10 rms
		Vertical	20~100 100~300 300~2000 Overall	+6 dB/octave 00 g^2/Hz −3 dB/octave ≥10 g
	RA	Horizontal	20~100 100~300 300~2000 Overall	+6 dB/octave 00 g^2/Hz −3 dB/octave ≤10 rms
		Vertical	20~100 100~300 300~2000 Overall	+6 dB/octave 00 g^2/Hz −3 dB/octave ≥10 g
Low-level random vibration test	TA/RA	All directions	5~2000	0.5 g (Uniformly distributed)
Shock test	TA/RA	All directions	~8000 Hz	Max 350 g
Thermal vacuum test	TA/RA	-	-	−00 ~ +00 °C

5.1. Vibration Test Considering Quasi-Static, Sinusoidal and Random Vibrational Load During the Launch Process

The structural integrity of the transmitting and receiving antenna assemblies against the quasi-optimal load determined by the mass acceleration curve was verified by a sine burst test [26]. The sine burst test is a test method that verifies the structural integrity against quasi-static acceleration using a vibration exciter. The test is conducted by exciting the specimen with a frequency less than one-third of the vibration mode frequency of the specimen and an acceleration that complies with the quasi-static test specifications. Several low-level random vibration tests are performed for each axis, and the primary principal vibration mode frequency in each direction is determined from the results of the first low-level random vibration test among the tests for each axis of the transmitting and

receiving antenna sections. As shown in Figure 13, the transmitting and receiving antenna sections satisfy the frequency requirements for avoiding interference with the vibration mode of the satellite in each direction.

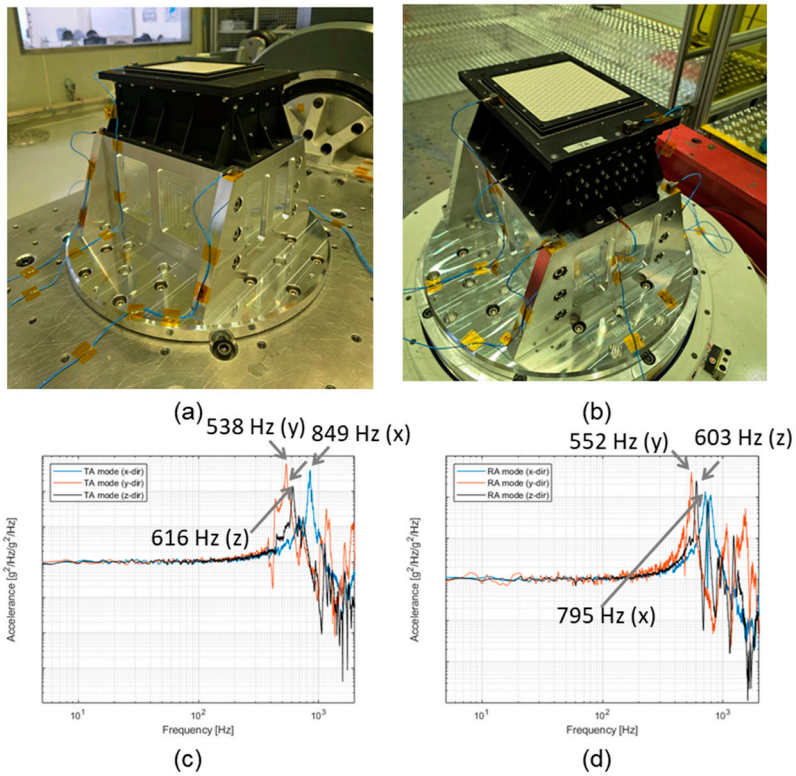


Figure 13. Evaluation of the vibrating mode frequency using the low-level random vibration test of transmitting antenna (TA) and receiving antenna (RA) assemblies for x, y, and z directions; test configuration of the (**a**) horizontal and (**b**) vertical conditions; the accelerance, which is the frequency response function of the acceleration measured in the (**c**) TA and (**d**) RA.

Generally, pass/fail criteria for environmental testing of satellite payloads are divided into three categories:

i. Whether the load delivered to the payload satisfies the test specification.
ii. Whether there were any structural changes in the prototype after each test.
iii. Whether there were any functional changes in the prototype after each test.

Figure 14 shows the vibration test results for the transmitting and receiving antenna assemblies. Figure 14a,b show the sine burst test results for the transmitting and receiving antenna assemblies. As mentioned earlier, the sine burst test is conducted by applying a load exceeding the test specifications 5 to 10 times at a frequency less than 1/3 of the first natural frequency. While excitation at a frequency less than 1/3 of the first natural frequency is necessary to maintain a distance from the prototype's first mode frequency during the test, sudden excitation at too high a frequency can strain the RA and TA [27]. Excitation at too low a frequency can result in vibration displacements that increase inversely proportional to the square of the excitation frequency. Therefore, in this study, the excitation frequency of the sine burst test was selected as 20 Hz, and the sine burst test was performed under the conditions corresponding to the test specifications. Figure 14c–f show that the input loads of the sine wave vibration test and the random vibration test of RA and TA for each direction fall within the tolerance line.

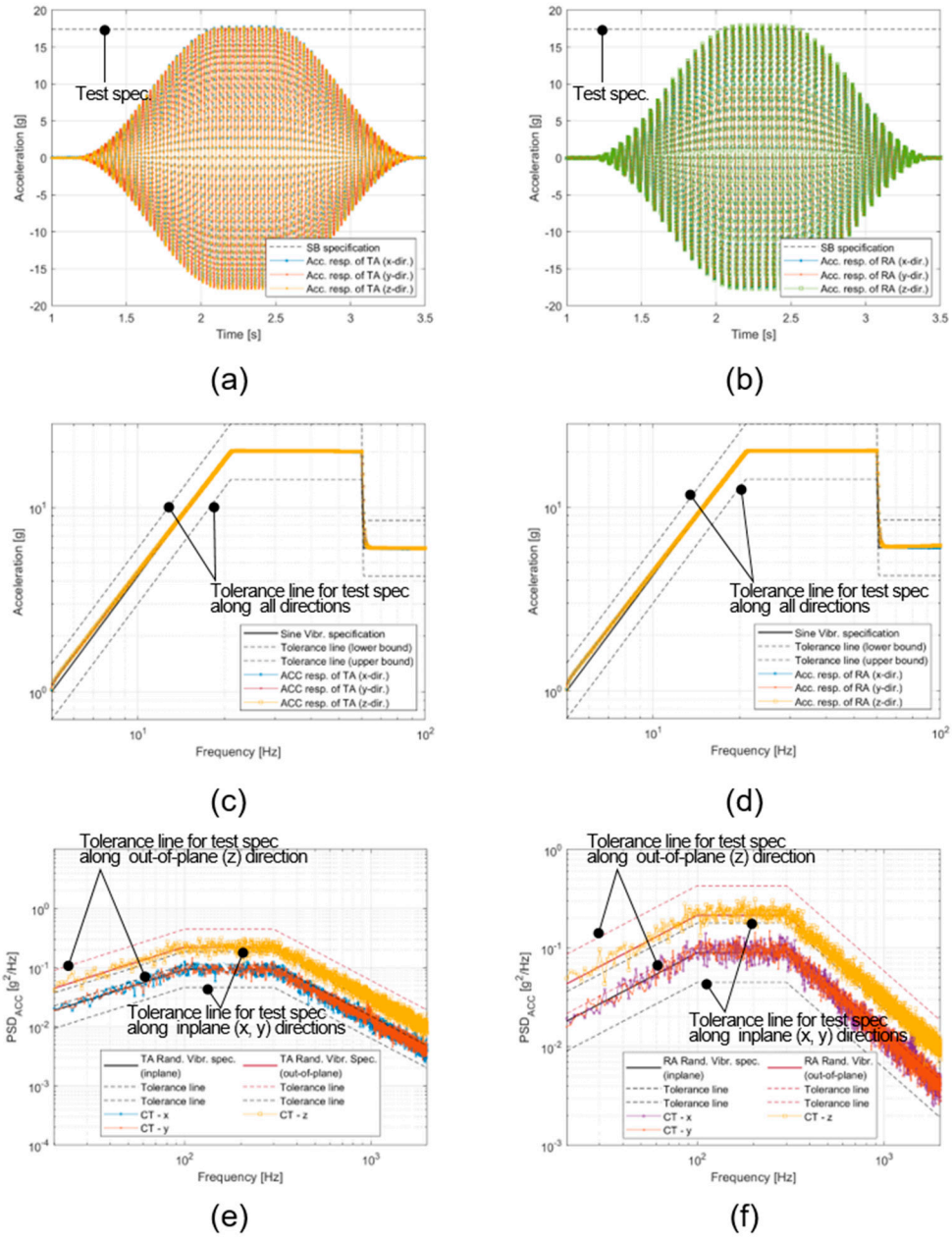


Figure 14. Result of the vibration test of the transmitting antenna (TA) and receiving antenna (RA) assemblies: Sine burst test of (**a**) TA and (**b**) RA for each direction; sine vibration test of (**c**) TA and (**d**) RA; random vibration test of (**e**) TA and (**f**) RA

To determine whether there were structural changes in the RAA and TAA after each test, low-level random vibration tests were conducted to compare the natural frequencies and response changes of the first modes in each first direction. By comparing the results of the pre-test and post-test for each load, if the frequency and response changes were less than 5% and 10%, respectively, it can be determined that there were no structural changes before and after each test. Table 3 shows that the vibration mode characteristics of the TA and RA identified in the pre-test and post-test for each test were sufficiently small.

Table 3. Change of the frequency (f-shift) and amplitude (a-shift) measured in the low-level random vibration test of transmitting antenna (TA) and receiving antenna (RA) assemblies before/after each main level vibration test for all directions.

DUT	Test	Direction	Frequency [Hz] (Before/After)	Amplitude (Before/After)	F-Shift [%]	A-Shift [%]	Results
TA	Sine burst	X	849/849	19.46/19.32	0.00	0.72	PASS
		Y	538/539	25.54/25.21	0.19	1.31	PASS
		Z	616/612	14.01/15.31	0.65	8.49	PASS
	Sine vibration	X	848/850	19.71/18.68	0.24	2.62	PASS
		Y	539/539	25.04/24.78	0.00	1.05	PASS
		Z	512/511	16.31/15.86	0.16	3.47	PASS
	Random vibration	X	846/847	20.97/19.88	0.12	5.48	PASS
		Y	534/533	26.29/26.77	0.19	1.79	PASS
		Z	603/603	12.60/1.78	0.00	6.96	PASS
RA	Sine burst	X	795/796	17.79/17.59	0.13	1.12	PASS
		Y	552/550	20.08/19.94	0.36	0.70	PASS
		Z	603/603	32.44/31.22	0.00	0.76	PASS
	Sine vibration	X	795/795	17.65/17.67	0.00	0.11	PASS
		Y	551/551	20.06/19.64	0.00	2.09	PASS
		Z	603/603	30.97/30.54	0.00	1.39	PASS
	Random vibration	X	796/796	16.27/15.98	0.00	1.78	PASS
		Y	547/546	19.73/19.86	0.18	0.66	PASS
		Z	600/597	24.68/22.04	0.50	10.70	PASS

5.2. Thermal Vacuum Test of the Transmitting Aantenna (TA) and Receiving Antenna (RA) Assemblies

This chapter covers thermal vacuum testing of the transmitting and receiving antenna assemblies. Thermal vacuum testing allows for the thermal stability of the payload against rapid temperature changes in the orbital environment. Because the test temperature ranges for the transmitting and receiving antenna assemblies are identical, the tests were conducted simultaneously. Similar to the vibration test, Figure 15 shows the results of the thermal cycle/thermal vacuum test for the transmitting and receiving antenna assemblies. As shown in Figure 15a,b, both antenna sections were tested simultaneously to save time and cost because they were tested within the same temperature range. The temperature reference point received from the satellite system is located at the interface between the satellite panel and the payload. For payload-level thermal environmental testing, the temperature reference point is the interface between the payload and the test zig. Figure 15c,d show the temperature/pressure profiles of the thermal cycle test and the thermal vacuum test, respectively. While thermal cycle testing is not mandatory during the payload qualification process, only one cycle is conducted to quickly determine whether the payload can function under both high and low temperatures. If all payloads function properly during the thermal cycle test, the thermal vacuum test is conducted. As shown in Figure 15d, health checks are performed under vacuum and room temperature conditions, and temperature transitions begin. The first cycle of thermal vacuum testing includes a power on/off test and a health check, followed by a health check in the eighth cycle. After the final health check in the room temperature/vacuum environment, normal operation is confirmed, concluding qualification for the orbital environment. The surface of the two antennas was treated by applying a black paint designed as Aeroglaze Z307, which provides a higher emissivity compared to that of the generally used black anodizing process, thereby enhancing the radiative heat dissipation performance of the payload.

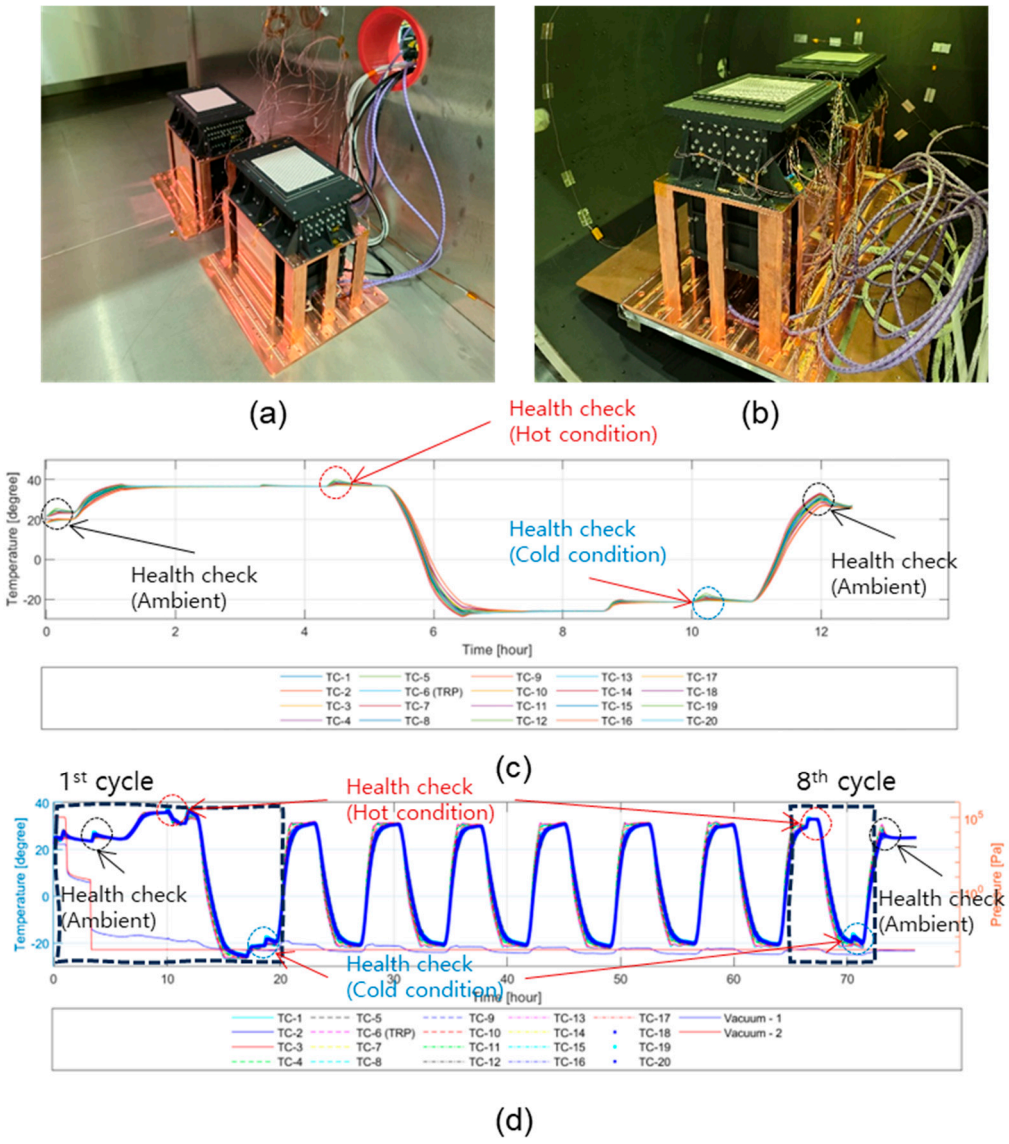


Figure 15. Thermal cycling (TC) and thermal vacuum (TV) tests of the transmitting antenna (TA) and receiving antenna (RA) assemblies: Experimental configuration of (**a**) TC and (**b**) TV tests; the time history of (**c**) temperature measured at TC test and (**d**) temperature and pressure measured at TV test.

5.3. Shock Test of the Transmitting Antenna (TA) and Receiving Antenna (RA) Assemblies

This chapter covers the shock tests for the transmitting and receiving antenna assemblies. These tests verify the payload's survivability against impact loads resulting from satellite launch and solar panel deployment during mission orbit. Shock tests for the transmitting and receiving antenna assemblies are conducted using a shock tester, applying shock loads that meet the test specifications once in each direction. The pass/fail criteria for the payload shock test are as follows:

i. Whether the impact test was performed with a load appropriate to the test specifications.
ii. Whether the function/performance of the transmitting/receiving antenna section is normally implemented after the impact test.

Figure 16 shows the shock test configuration for the transmitting and receiving antenna sections. Figure 16a–c show the experimental setups for the horizontal and vertical directions of the transmit antenna section. Since the transmitting and receiving antenna assemblies have identical zig interfaces and similar mass properties, the shock test is conducted using the same test fixture. Furthermore, since KTL's gunfire tester applies

shocks to the test subject in the same direction, the shock test fixture was designed and manufactured to allow the test specimen to be installed along the test axis. Figure 16a,b show the test configurations for the horizontal and vertical directions of the two antenna assemblies. The shock test for the transmit/receive antenna sections is conducted using the same procedure, and after the shock test for each layer, a functional/performance test is performed to determine the pass/fail criteria for each direction. Figure 16c,d show the shock test results for the transmitting and receiving antenna sections, respectively. The response of the control accelerometer attached to the shock test cradle shows that the test was performed according to the shock test specifications defined in Table 1.

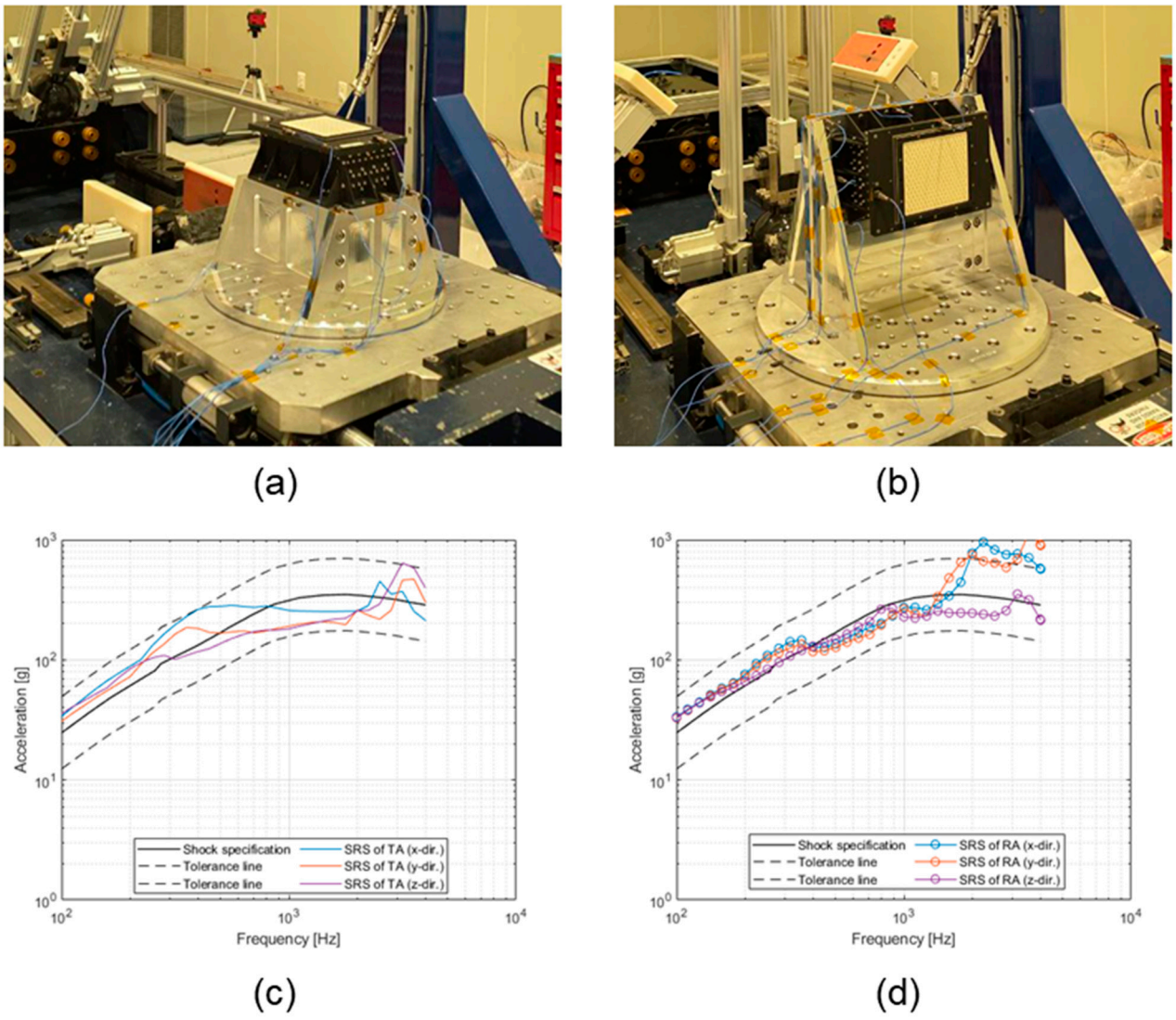


Figure 16. Shock test of the transmitting antenna (TA) and the receiving antenna (RA): Experimental setup of TA for (**a**) inplane and (**b**) out of plane directions (the same with the configuration of TA); SRS response measured in the shock test of (**c**) TA and (**d**) RA.

Table 4 presents the results of functional tests conducted during environmental testing of the transmitting and receiving antenna assemblies. Functional tests of the transmitting and receiving antenna assemblies were conducted after the structural environmental tests for each axis, after the impact tests for each axis, and during the thermal vacuum test. The results of the functional tests conducted at each stage indicate that no functional defects occurred in the transmitting and receiving antenna assemblies during the environmental tests.

Table 4. Result of the functional test of the transmitting antenna (TA) and the receiving antenna (RA) assemblies during the structural/thermal environmental and shock tests.

DUT	Function Test	Vibration Test		Thermal Test		Shock Test	
		Before	After	Before	After	Before	After
TAA	Power input	PASS	PASS	PASS	PASS	PASS	PASS
	RS-422	PASS	PASS	PASS	PASS	PASS	PASS
	FPGA	PASS	PASS	PASS	PASS	PASS	PASS
	PROM	PASS	PASS	PASS	PASS	PASS	PASS
	TCM Temp.	PASS	PASS	PASS	PASS	PASS	PASS
	TRF Temp.	PASS	PASS	PASS	PASS	PASS	PASS
	UCM Temp.	PASS	PASS	PASS	PASS	PASS	PASS
	TRSA Temp.	PASS	PASS	PASS	PASS	PASS	PASS
	TRSA PLL	PASS	PASS	PASS	PASS	PASS	PASS
RAA	Power input	PASS	PASS	PASS	PASS	PASS	PASS
	RS-422	PASS	PASS	PASS	PASS	PASS	PASS
	FPGA	PASS	PASS	PASS	PASS	PASS	PASS
	PROM	PASS	PASS	PASS	PASS	PASS	PASS
	RCM Temp.	PASS	PASS	PASS	PASS	PASS	PASS
	RRF Temp.	PASS	PASS	PASS	PASS	PASS	PASS
	DCM Temp.	PASS	PASS	PASS	PASS	PASS	PASS
	RRSA Temp.	PASS	PASS	PASS	PASS	PASS	PASS
	RRSA PLL	PASS	PASS	PASS	PASS	PASS	PASS

6. Conclusions

In this study, we propose a systematic qualification process for a planar phased array antenna employing cavity-coupled slot-patch radiating elements for Ka-band low-Earth orbit communication satellites and present the results. To verify the reliability of the soldering process for large-scale array antennas, 36- and 48-scaled reduced models of the transmitting and receiving antenna assemblies were fabricated, respectively. These scale models were subjected to space-based environmental testing, including vibration, shock, and thermal cycle tests. Passive return loss measurements and visual inspections were performed before and after each test, confirming the structural integrity and electrical performance of the antenna assembly. After all space-based environmental tests, micro-section analysis of the solder joints confirmed the reliability of manual soldering in space environments. Next, we developed assembly support equipment to control the high bonding pressure generated by spring-loaded bullet-mate connectors used to connect the antenna module and the RF integrated module and to ensure precise alignment of the array elements. Using this, we assembled the full-array transmitting and receiving antenna assemblies and then performed space environment tests, including structural environmental tests, thermal environmental tests, and impact tests. Functional tests were performed before and after each test to confirm that the structural and functional performance met the requirements under all test conditions. This study covers the systematic development and certification procedures for the development of large-scale planar array antennas for communication satellites, from soldering process certification → development of assembly support equipment → environmental tests of the transmit/receive antenna sections. In particular, the pre-verification strategy for process certification verification using a scaled-down model enabled the early detection of design defects and process optimization, effectively reducing development risks. The systematic verification method presented in this study includes the process of assembling a large number of antenna arrays using a bullet mate connector without gain loss. Therefore, the series of processes, ranging from incremental scaling of the antenna model and assembly of the antenna assembly to environmental testing of the

antenna assembly, is expected to be applicable to the development of antennas of various sizes to be used in future Ka-band low-orbit communication satellite constellations and contribute to ensuring the reliability of next-generation satellite communication systems.

Author Contributions: Conceptualization, K.C.K.; methodology, H.-G.K., S.-J.L. and B.-G.Y.; software, J.B., E.-T.J. and W.-S.C.; validation, J.-H.C., H.K., H.M. and H.K.; formal analysis, H.-G.K. and J.B.; investigation, E.-T.J. and W.-S.C.; resources, J.-I.C., J.C. and W.-S.L.; data curation, W.-S.C., E.-T.J., J.B., I.P., M.L. and H.-G.K.; writing—original draft preparation, H.-G.K. and J.B.; writing—review and editing, E.-T.J., I.P., M.L. and W.-S.C.; visualization, H.-G.K.; supervision, J.-H.C., K.Y.P., K.C.K. and K.H.; project administration S.-J.L., J.-H.C., B.K., K.Y.P. and K.C.K.; funding acquisition: S.-J.L., B.-G.Y., J.-H.C., K.Y.P. and K.C.K. All authors have read and agreed to the published version of the manuscript.

Funding: This work was supported by the Agency for Defense Development by the Korean Government (915082202).

Institutional Review Board Statement: Not applicable.

Informed Consent Statement: Not applicable.

Data Availability Statement: All data are in the paper; there are no additional data.

Conflicts of Interest: Authors Hyun-Guk Kim, Jiye Bak, Seong-Ju Lee, Eun-Tae Jung, Woon-Sung Choi, Byeong-Gil Yu, Jaekark Choi, Jung-Il Cho, Won-Seok Lee, Insung Park, Hansol Min, Hyun Koh and Myeongjae Lee were employed by the company Hanwha Systems. The remaining authors declare that the research was conducted in the absence of any commercial or financial relationships that could be construed as a potential conflict of interest.

Abbreviations

The following abbreviations are used in this manuscript:

TA	Transmitting antenna
RA	Receiving antenna
LLRVT	Low level random vibration test
TVac	Thermal-vacuum test
TRM	Transmitting reduced model
RRM	Receiving reduced model
LEO	Low earth orbit
ISL	Inter-satellite link
FRF	Frequency response function
CTE	Coefficient of thermal expansion
IMC	Inter-metallic compound
TC	Thermal cycling test
PRL	Passive return loss
VI	Visual inspection

References

1. Curzi, G.; Modenini, D.; Tortora, P. Large constellations of small satellites: A survey of near future challenges and missions. *Aerospace* **2020**, *7*, 133. [CrossRef]
2. Kodheli, O.; Lagunas, E.; Maturo, N.; Sharma, S.K.; Shankar, B.; Montoya, J.F.M.; Duncan, J.C.M.; Spano, D.; Chatzinotas, S.; Kisseleff, S.; et al. Satellite Communications in the New Space Era: A Survey and Future Challenges. *IEEE Commun. Surv. Tutor.* **2021**, *23*, 70–109. [CrossRef]
3. MarketsandMarkets. Communication Small Satellite Market Worth $18.34 Billion by 2030 [Press Release]. PR Newswire. 7 January 2026. Available online: https://www.marketsandmarkets.com/PressReleases/communication-small-satellite.asp (accessed on 11 March 2026).

4. Jiang, R.; Liang, W.; Wang, L.; Su, H.; Zhang, Y.; Jiang, T.; Du, J.; Zhang, A. Microvibration Testing and Decoupling for Space Payloads with Large Inertia, High Stiffness, and Discrete Interfaces. *Sensors* **2025**, *25*, 7352. [CrossRef] [PubMed]
5. De la Cruz, M.T.; Gamboa, R.G.P.; Dalisay, J.D.E.; Raguindin, R.K.M.; Magdaluyo, E.R. Development and Feasibility Assessment of a Sequential Antenna Deployment System Based on Fiber-Reinforced Shape Memory Polymer Composites. *Polymers* **2025**, *17*, 2797. [CrossRef] [PubMed]
6. Zhou, H.; Jong, M.; Lo, M.G. Evolution of Satellite Communication Antennas on Mobile Ground Terminals. *Int. J. Antennas Propag.* **2015**, *2015*, 436250. [CrossRef]
7. Ortiz, F.; Baeza, V.M.; Garces-Socarras, L.M.; Vásquez-Peralvo, J.A.; Gonzalez, J.L.; Fontanesi, G.; Lagunas, E.; Querol, J.; Chatzinotas, S. Onboard Processing in Satellite Communications Using AI Techniques: A Survey. *Aerospace* **2023**, *10*, 101. [CrossRef]
8. Rao, S.K. Advanced Antenna Technologies for Satellite Communications Payloads. *IEEE Trans. Antenna Propag.* **2015**, *63*, 1205–1217. [CrossRef]
9. Perera, S.; Zhang, Y.; Zrnic, D.; Doviak, R. Electromagnetic simulation and alignment of dual-polarized array antennas in multi-mission phased array radars. *Aerospace* **2017**, *4*, 7. [CrossRef]
10. Usmani, W.U.; Chietera, F.P.; Mescia, L. Flexible Phased Antenna Arrays: A Review. *Sensors* **2025**, *25*, 4690. [CrossRef] [PubMed]
11. Anim, K.; Lee, J.N.; Jung, Y.B. High-Gain Millimeter-Wave Patch Array Antenna for Unmanned Aerial Vehicles Application. *Sensors* **2021**, *21*, 3914. [CrossRef] [PubMed]
12. Kang, W.; Lim, T.H.; Kim, Y.; An, S.; Joo, J.H.; Byun, G. Design of a Compact Indirect Slot-Fed Wideband Patch Array with an Air SIW Cavity for a High Directivity in Missile Seeker Applications. *Appl. Sci.* **2022**, *12*, 9569. [CrossRef]
13. Rafal, G. Planar Antennas for Ka-Band Space Applications. Ph.D. Thesis, École Polytechnique Fédérale de Lausanne (EPFL), Lausanne, Switzerland, 2013.
14. *ECSS-Q-ST-70-08C*; Manual Soldering of High-Reliability Electrical Connections. European Cooperation for Space Standardization (ECSS): Noordwijk, The Netherlands, 2014.
15. *ECSS-Q-ST-70-38C*; High-Reliability Soldering for Surface-Mount and Mixed Technology. European Cooperation for Space Standardization (ECSS): Noordwijk, The Netherlands, 2018.
16. *GSFC-STD-7000A*; General Environmental Verification Standard (GEVS) for GSFC Flight Programs and Projects. Goddard Space Flight Center, NASA: Greenbelt, MD, USA, 2013.
17. *ECSS-E-ST-10-03C*; Space Engineering—Testing. European Cooperation for Space Standardization (ECSS): Noordwijk, The Netherlands, 2022.
18. Abdullah, F.; Okuyama, K.; Fajardo, I.; Urakami, N. Experimental Study on Thermal Cycling Effects in Lead-Free Solder Joints for Space Electronics. *Aerospace* **2020**, *7*, 35. [CrossRef]
19. Raffa, L.S.; Ryall, M.; Cairns, I.; Bennett, N.S.; Clemon, L. Investigating the Performance of a Heat Sink for Satellite Avionics Thermal Management: From ground-level testing to space-like conditions. *Int. J. Heat Mass Transf.* **2025**, *9*, 35. [CrossRef]
20. Skytrac. The Differences, Strengths, and Weaknesses of LEO and GEO Satellite Networks. Available online: https://www.skytrac.ca/resources/magazine/skytrac-satcomseries-the-differences-strengths-and-weaknesses-of-leo-and-geo-satellites/ (accessed on 11 January 2026).
21. Lu, F.; Jiang, Y.; Wang, H.; Zhao, P.; Wei, H.; Ma, B.; Ma, C. System demonstrations of Ka-band 5-Gbps data transmission for satellite applications. *Int. J. Satell. Commun. Netw.* **2021**, *40*, 204–217. [CrossRef]
22. Pratt, S.R.; Raines, R.A.; Fossa, C.E.; Temple, M.A. An operational and performance overview of the IRIDIUM low earth orbit satellite system. *IEEE Commun. Surv.* **1999**, *2*, 2–10. [CrossRef]
23. Kim, H.-G.; Bak, J.; Cho, J.; Lee, S.-J.; Lee, W.-S.; Park, K.-Y.; Kim, K.-C. Structural Analysis of Digital Transceiver Unit (DTU) for 400 kg-Class Communication Satellite Considering Launch Environment. *IEEE Access* **2025**, *13*, 151316–151326. [CrossRef]
24. Bak, J.; Kim, H.-G.; Cho, J.; Lee, S.-J.; Lee, W.-S.; Park, K.-Y.; Kim, K.-C. Thermal Analysis of Digital Transceiving Unit (DTU) for 400 kg-Class Communication Satellite Considering On-Orbit Environment. *IEEE Access* **2025**, *13*, 142571–142582. [CrossRef]
25. Bak, J.; Kim, H.; Lee, S.J.; Jung, E.T.; Park, K.Y.; Kim, K.C. Environment Test for Soldering Process Qualification of Reduced Module of Communication Satellite Antenna. *Trans. Korean Soc. Mech. Eng. A*, 2026, *submitted*.
26. Trudberts, M. *Mass Acceleration Curve for Spacecraft Structural Design*; JPL-D-5882; NASA Jet Propulsion Laboratory: Pasadena, CA, USA, 1989.
27. Johnson, D. *Best Practice for Use of Sine Burst Testing*; NASA Engineering and Safety Technical Bulletin No. 15-02; NASA: Hampton, VA, USA, 2015. Available online: https://ntrs.nasa.gov/citations/20240000431 (accessed on 3 March 2026).

Disclaimer/Publisher's Note: The statements, opinions and data contained in all publications are solely those of the individual author(s) and contributor(s) and not of MDPI and/or the editor(s). MDPI and/or the editor(s) disclaim responsibility for any injury to people or property resulting from any ideas, methods, instructions or products referred to in the content.